IEEE Access
Multidisciplinary | Rapid Review | Open Access Journal

Received 24 October 2023, accepted 16 November 2023, date of publication 28 November 2023,
date of current version 1 December 2023.

Digital Object Identifier 10.1109/ACCESS.2023.3336279

RESEARCH ARTICLE

A Multi-Input Multi-Output Model Predictive Direct Torque Control for Dual Mechanical Port Machine

HAMED BIZHANI[1,2], (Member, IEEE), LAZHAR BEN-BRAHIM[1], (Life Senior Member, IEEE), ADEL GASTLI[1], (Senior Member, IEEE), NASSER AL-EMADI[1], (Senior Member, IEEE), AND MOHAMED DJEMAI[3,4], (Senior Member, IEEE)

[1]Department of Electrical Engineering, Qatar University, Doha, Qatar
[2]Institute of Control and Industrial Electronics, Faculty of Electrical Engineering, Warsaw University of Technology, 00-665 Warsaw, Poland
[3]LAMIH, UPHF, INSA HdF, 59313 Valenciennes, France
[4]Quartz, ENSEA, 95000 Cergy, France

Corresponding author: Lazhar Ben-Brahim (brahim@qu.edu.qa)

This work was supported in part by Qatar University under Grant IRCC-2022-543, and in part by the Qatar National Library.

ABSTRACT In this paper, a multi-input multi-output (MIMO) model predictive direct torque control (MPDTC) strategy for a dual mechanical port machine (DMPM) is proposed. A MIMO state space model is developed, incorporating the electromagnetic interaction between the stator, inner rotor, and outer rotor of the DMPM. The prediction model is then derived to adjust the currents of stator and inner rotor windings, enabling independent control of the electromagnetic torques of the mechanical ports. Compared to single-input single-output based MPC and PI-based field-oriented control strategies, the proposed approach effectively mitigates the undesired electromagnetic interactions, guaranteeing smooth speed control of both mechanical ports. The simulation results carried out by MATLAB/Simulink verify the precise performance of the DMPM in different operating modes. The Hardware-in-the-Loop results further confirm that the proposed direct torque control not only regulates the inner and outer rotor independently, but can also be executed in real-time without posing any computational burden on the processor. A sensitivity analysis for evaluating the performance of the proposed strategy in the presence of variations in the electrical parameters of the DMPM is also provided.

INDEX TERMS Dual mechanical port machine, model predictive control, direct torque control, multi-input multi-output systems, hardware in the loop.

I. INTRODUCTION

Electrical machines (EMs) are the most critical propulsion component in different applications, such as wind energy systems and electric vehicles. Various types of EMs have already been proposed by researchers and engineers to cover specific needs of these applications. Induction and permanent magnet synchronous machines with a single mechanical port are the most well-known ones in the industry. Over the past decade, however, the concept of dual mechanical ports machines (DMPM) was introduced by the researchers [1], [2]. Due to its smaller size and cost-effectiveness, the DMPM has found applications in various fields, such as pure electric vehicle [3], [4], [5], hybrid electric vehicle [6], [7], [8], [9], wind energy systems [10], [11], [12], and others [13].

Unlike traditional EMs, which can adjust only one mechanical output using one or two electrical inputs, a DMPM offers the unique capability of controlling two mechanical ports using just one or two electrical ports. Depending on the location of the stator and rotor, as well as the type of the rotor, such as squirrel cage, permanent magnet (PM), or wound, various configurations for creating a DMPM are feasible [5]. A DMPM with an electric port in the stator, a wound inner rotor, and a PM outer rotor, provides two control freedoms for independent control of the mechanical ports, leading to improved dynamic performance in hybrid electric vehicles [7]. However, achieving independent control in DMPMs is challenging due to the electromagnetic

The associate editor coordinating the review of this manuscript and approving it for publication was Yuh-Shyan Hwang.

interactions between magnetic fields of the stator, inner rotor, and PM rotor, where the variations in the torque and speed of the inner rotor inversely affect the dynamic performance of the outer rotor and vice versa. Simple field-oriented control (FOC) strategy is developed in [6], [8], [9], and [14], without considering the magnetic fields interactions. In [15], a dc-field winding is added into the DMPM to create a decoupling bridge between the stator and inner rotor in a way that the stator flux can be separately modulated while maintaining the rotor flux linkage. A torque controller considering the electromagnetic coupling is then developed that combines the stator, dc-field, and inner rotor currents for minimizing the copper and iron losses in every operating condition. In [16], the PM rotor is replaced by a squirrel cage rotor to lower the machine's cost and to improve the thermal tolerance. Considering the magnetic coupling between stator and outer rotor, and inner and outer rotors, an independent control algorithm for controlling both rotors is presented. In [17], decoupling terms are feed-forwarded into the conventional field oriented control to minimize the magnetic interactions. Using a special design in [18], the flux coupling between two windings located in the stator of a brush-less DMPM is mitigated, making the use of conventional FOC feasible.

Owing to the significant developments in the processor manufacturing, the model predictive control (MPC) has become much more applicable for electric drives [19]. Compared with the conventional control strategies, the MPC can easily control the nonlinear and multi-input multi-output (MIMO) systems, while considering the system's constraints and uncertainties. For controlling the DMPM, two finite-set model predictive control (FS-MPC) strategies are reported in [20] and [21], where two independent MPC algorithms are employed for independent speed control of the inner and outer rotors of a DMPM. For this purpose, the dynamic equations of the inner and outer machines are first used to create two separate single-input single output (SISO) prediction models. By neglecting the mutual effects of electrical ports, two completely independent cost functions are developed to individually evaluate the feasible switching set of each inverter and to obtain the optimum switching state in the next sampling instant. This leads to an unshaped speed adjustment of the DMPM. To offer the advantages of the model predictive control and at the same time removing the undesired interactions between ports, a multi-input multi-output based model predictive direct torque control (MPDTC) is proposed in this paper. Instead of controlling the stator and inner rotors' inverters with two independent FS-MPC loops, a comprehensive cost function containing the control variables of both outputs is defined so that the optimum switching states of both inverters are obtained simultaneously, while their undesired effects on the other output are taken into consideration. In other words, the two three-phase inverters are assumed to operate as a single six-leg inverter with $2^6 = 64$ feasible switching states. The dynamic equations of both inner and outer rotors are accordingly merged to create a MIMO prediction model. A multi-objective cost function containing the control objectives of both ports is also developed to find the optimum switching state that leads to an overall minimum cost function. Using this strategy, the mutual impact of inverters is considered so that the undesired electromagnetic interaction between mechanical ports can be effectively mitigated. Consequently, the precise and independent control of both mechanical ports is guaranteed. The performance of the proposed strategy in different operating modes is evaluated using MATLAB/Simulink. The real-time assessment of the proposed approach is also verified using Typhoon HIL 602 and dSPACE 1103 devices. Both simulation and hardware results are finally compared with the conventional FOC and SISO-based MPC strategies. A sensitivity analysis for evaluating the impacts of the electrical parameters on the performance of the proposed strategy is also reported.

In Section II, the application of DMPM in HEV is introduced and the dynamic model of the DMPM is presented. The multi-input multi-output state space of the DMPM is derived in Section III. The model predictive direct control strategy is then proposed in this section. Simulation results are given in Section IV. Hardware-in-the-loop results and real-time execution analysis are respectively provided in Section V and Section VI. Finally, a sensitivity analysis is developed in Section VII.

II. DMPM-BASED HYBRID ELECTRIC VEHICLE

A. DMPM APPLICATION IN HEVs

HEVs can be categorized into three groups based on their structures: series hybrid, parallel hybrid, and series-parallel hybrid [8]. Despite their more complex design, series-parallel HEVs combine the advantages of both series and parallel hybrids. Due to the presence of more energy flow paths and operating modes compared to other configurations, power management and control strategies become more intricate. To interface the Internal Combustion Engine (ICE) and two electrical machines (one serving as a motor and the other as a generator) with the vehicle's drive-train, a planetary gear set is employed. This arrangement enables the vehicle to achieve desirable speeds while ensuring the ICE operates within its most fuel-efficient speed range [7]. Consequently, the planetary gear set not only combines the driving power from the ICE and electric motor/generator, but also acts as a continuous variable transmission. However, the inclusion of two electrical machines, two power electronic inverters, and a set of planetary gearboxes makes the traction system more complex and increases its size. An alternative solution, the DMP machine, presents an opportunity to achieve all the functions and benefits offered by existing HEV technologies within a single, compact package as shown in Fig. 1. The DMP machine replaces the planetary gearbox and the two electric machines found in conventional series-parallel HEVs, simplifying their structures. Furthermore, this design eliminates the mechanical losses associated with the planetary gear.

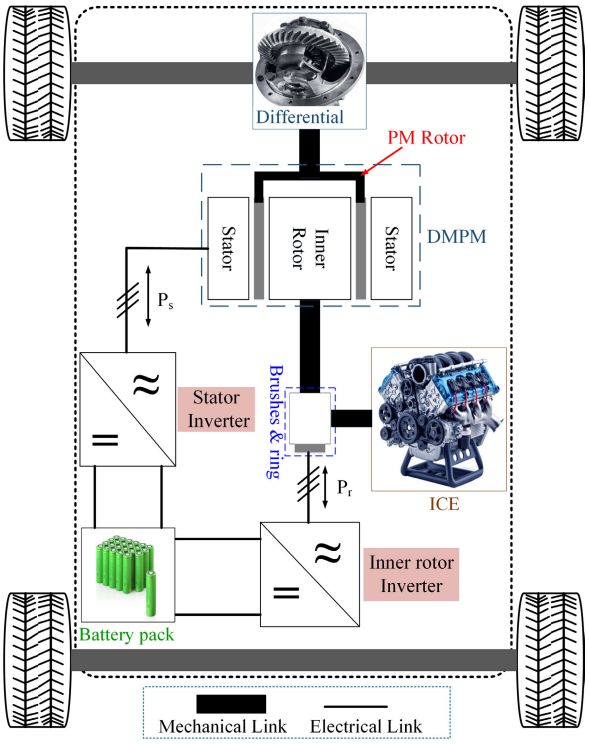

FIGURE 1. Application of a DMPM in hybrid electric vehicle.

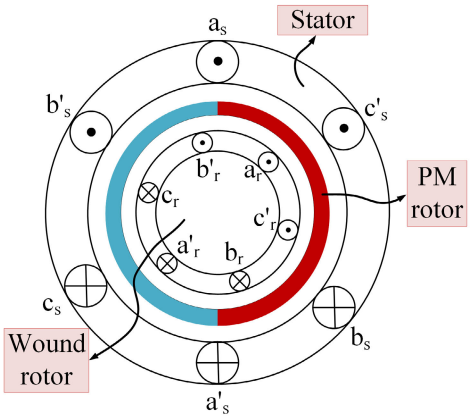

FIGURE 2. Cross section of a two-pole three-phase dual mechanical port machine with a wound inner rotor and a permanent magnet outer rotor.

B. DMPM DYNAMIC MODELING

The structure of a dual mechanical port machine is shown in Fig. 2. Although different configurations to create a dual rotor electric machine are feasible [5], a dual rotor machine containing two electrical ports, i.e., stator and inner rotor windings, and two mechanical ports named inner and outer rotors, is used in this study. According to the literature, the inner and outer rotors can be either a permanent magnet, squirrel cage, or wound rotor [5], [22], [23]. While a wound rotor might increase the losses and requires frequent maintenance due to the presence of the brushes, the inner and outer rotors are respectively considered wound and PM rotors in this paper to provide more control flexibility. In this case, the stator and inner rotor windings serve as input ports, individually connected to three-phase DC/AC inverters as depicted in Fig. 1. The inverters are responsible for adjusting the windings' voltages, ensuring that both mechanical ports can accurately track their reference values. The conventional controller for DMPM employs a field oriented control approach, where speed control of the inner and outer ports is conducted without considering the interactions between magnetic fields. This leads to unshaped speed control, where the variations in torque and speed of the inner rotor adversely affect the performance of the outer rotor, and vice versa. To address this limitation, a multi-input multi-output direct torque model with predictive control is proposed, which takes into account the undesired electromagnetic interactions between different ports. To achieve this, the prediction model of the DMPM machine is required. According to [1], [6], [7], [8] and [9], the dynamic model of the stator in the outer reference frame is represented as follows:

$$V_{qs} = r_s i_{qs} + \frac{d\lambda_{qs}}{dt} + \omega_{pm}\lambda_{ds} \tag{1}$$

$$V_{ds} = r_s i_{ds} + \frac{d\lambda_{ds}}{dt} - \omega_{pm}\lambda_{qs} \tag{2}$$

where V_{ds}, V_{qs}, i_{ds}, and i_{qs} are the stator voltage and current in the synchronous reference frame, ω_{pm} is the electrical speed of the outer rotor, and r_s is the stator resistance. λ_{ds} and λ_{qs} denote for the stator flux linkages in the synchronous reference frame and are obtained by:

$$\lambda_{ds} = L_{ds} i_{ds} + L_{md} i_{dr} + \lambda_m \tag{3}$$

$$\lambda_{qs} = L_{qs} i_{qs} + L_{mq} i_{qr} \tag{4}$$

where L_{ds} and L_{qs} are stator self-inductance for d- and q-axis, respectively, L_{md} and L_{mq} are mutual inductance between inner rotor and stator windings, and λ_m is the flux linkage produced by outer rotor. Similarly, the dynamic model for inner rotor can be also expressed by:

$$V_{qr} = r_r i_{qr} + \frac{d\lambda_{qr}}{dt} + (\omega_{pm} - \omega_r)\lambda_{dr} \tag{5}$$

$$V_{dr} = r_s i_{dr} + \frac{d\lambda_{dr}}{dt} - (\omega_{pm} - \omega_r)\lambda_{qr} \tag{6}$$

where V_r, i_r are the inner rotor voltage and current in the reference frame, ω_r is the electrical speed of the inner rotor, and r_r is the rotor resistance. λ_{dr} and λ_{qr} represent the rotor flux linkages in dq frame and are defined by:

$$\lambda_{dr} = L_{dr} i_{dr} + L_{md} i_{ds} + \lambda_m \tag{7}$$

$$\lambda_{qr} = L_{qr} i_{qr} + L_{mq} i_{qs} \tag{8}$$

where L_{dr} and L_{qr} are rotor self-inductance for d- and q-axis, respectively. The dynamic model for the mechanical ports are written as:

$$T_{e,pm} - T_{L,pm} = J_{pm}\frac{d\omega_{om}}{dt} + B_{pm}\omega_{pm} \tag{9}$$

$$T_{e,in} - T_{L,in} = J_{in}\frac{d\omega_{in}}{dt} + B_{in}\omega_{in} \tag{10}$$

where $T_{e,pm}$ and $T_{e,in}$ are the developed electromagnetic torques, J_{pm} and J_{in} are inertia, and B_{pm} and B_{in} are friction

coefficients for outer and inner rotors, respectively. The electromagnetic torques are then obtained as follows:

$$T_{e,pm} = \frac{3}{2} p \lambda_m (i_{qs} + i_{qr}) \tag{11}$$

$$T_{e,in} = \frac{3}{2} p (\lambda_m i_{qr} + \lambda_{ds} i_{qr} - \lambda_{qs} i_{dr}) \tag{12}$$

where p denotes the number of pole pairs. Considering the stator and rotor currents as the state variables and voltages as control variables, the electrical dynamic equations can be written as follows:

$$\begin{aligned} \frac{di_{qs}}{dt} = \frac{1}{\sigma_q L_{qs}} \Big[& V_{qs} - \gamma_{qr} V_{qr} - r_s i_{qs} + \gamma_{qr} r_r i_{qr} \\ & - i_{dr} \left(\omega_{pm} L_{md} - \gamma_{qr} L_{dr} (\omega_{pm} - \omega_r) \right) \\ & - i_{ds} \left(\omega_{pm} L_{ds} - \gamma_{qr} L_{md} (\omega_{pm} - \omega_r) \right) \\ & - \lambda_m \left(\omega_{pm} - \gamma_{qr} (\omega_{pm} - \omega_r) \right) \Big] \end{aligned} \tag{13}$$

$$\begin{aligned} \frac{di_{ds}}{dt} = \frac{1}{\sigma_d L_{ds}} \Big[& V_{ds} - \gamma_{dr} V_{dr} - r_s i_{ds} + \gamma_{dr} r_r i_{dr} \\ & + i_{qr} \left(\omega_{pm} L_{mq} - \gamma_{dr} L_{qr} (\omega_{pm} - \omega_r) \right) \\ & + i_{qs} \left(\omega_{pm} L_{qs} - \gamma_{dr} L_{mq} (\omega_{pm} - \omega_r) \right) \Big] \end{aligned} \tag{14}$$

$$\begin{aligned} \frac{di_{qr}}{dt} = \frac{1}{\sigma_q L_{qr}} \Big[& V_{qr} - \gamma_{qs} V_{qs} - r_r i_{qr} + \gamma_{qs} r_s i_{qs} \\ & - i_{ds} \left((\omega_{pm} - \omega_r) L_{md} - \gamma_{qs} L_{ds} \omega_{pm} \right) \\ & - i_{dr} \left((\omega_{pm} - \omega_r) L_{dr} - \gamma_{qs} L_{md} \omega_{pm} \right) \\ & - \lambda_m \left((\omega_{pm} - \omega_r) - \gamma_{qs} \omega_{pm} \right) \Big] \end{aligned} \tag{15}$$

$$\begin{aligned} \frac{di_{dr}}{dt} = \frac{1}{\sigma_d L_{dr}} \Big[& V_{dr} - \gamma_{ds} V_{ds} - r_r i_{dr} + \gamma_{ds} r_s i_{ds} \\ & + i_{qs} \left((\omega_{pm} - \omega_r) L_{mq} - \gamma_{ds} L_{qs} \omega_{pm} \right) \\ & + i_{qr} \left((\omega_{pm} - \omega_r) L_{qr} - \gamma_{ds} L_{mq} \omega_{pm} \right) \Big] \end{aligned} \tag{16}$$

where

$$\sigma_q = (1 - \frac{L_{mq}}{L_{qs} L_{qr}}), \quad \sigma_d = (1 - \frac{L_{md}}{L_{ds} L_{dr}})$$

$$\gamma_{qs} = \frac{L_{mq}}{L_{qs}}, \quad \gamma_{ds} = \frac{L_{md}}{L_{ds}}, \quad \gamma_{qr} = \frac{L_{mq}}{L_{qr}}, \quad \gamma_{dr} = \frac{L_{md}}{L_{dr}}$$

III. MODEL PREDICTIVE CONTROL

The FS-MPC predicts the control variables for all feasible switching states within a specific prediction horizon. To achieve this, the dynamic model of the system is first discretized, and prediction models in terms of the input variables and control variables at the current instant (k) are derived to predict the objective variables over the next sampling period ($k + 1$). A pre-defined cost function, containing the cumulative error between the predicted control variables and their reference values over the prediction horizon, is then evaluated for each switching state. Finally, the switching state resulting in the minimum cost is selected and applied at the next sampling time ($k + 1$). The schematic of the proposed model predictive direct torque control for a DMPM based HEV is depicted in Fig. 3.

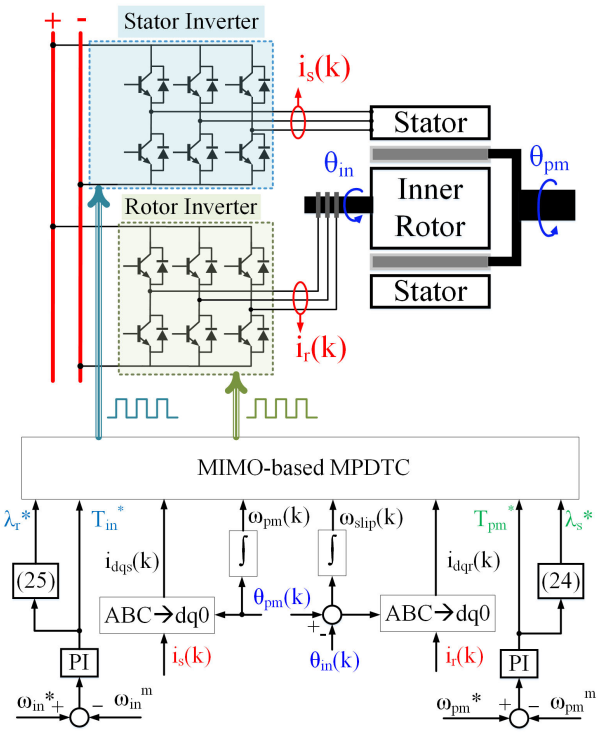

FIGURE 3. Model predictive direct torque control scheme for DMPM based HEV.

A. PREDICTION MODEL

To implement the direct torque control using the MPC approach, it is essential to define prediction models for the electrical state variables of the system. Utilizing the Euler approximation, the prediction model of the system for predicting the state variables in the next sampling period is obtained as follows:

$$\begin{aligned} & i_{qs}(k+1) \\ & = \Big[V_{qs}^* - \gamma_{qr} V_{qr}^* - r_s i_{qs}(k) + \gamma_{qr} r_r i_{qr}(k) \\ & \quad - i_{dr}(k) \Big(\omega_{pm} L_{md} - \gamma_{qr} L_{dr} \left(\omega_{pm}(k) - \omega_r(k) \right) \Big) \\ & \quad - i_{ds}(k) \Big(\omega_{pm}(k) L_{ds} - \gamma_{qr} L_{md} \left(\omega_{pm}(k) - \omega_r(k) \right) \Big) \\ & \quad - \lambda_m \Big(\omega_{pm}(k) - \gamma_{qr} \left(\omega_{pm}(k) - \omega_r(k) \right) \Big) \Big] \times \frac{T_s}{\sigma_q L_{qs}} \\ & \quad + i_{qs}(k) \end{aligned} \tag{17}$$

$$\begin{aligned} & i_{ds}(k+1) \\ & = \Big[V_{ds}^* - \gamma_{dr} V_{dr}^* - r_s i_{ds}(k) + \gamma_{dr} r_r i_{dr}(k) \\ & \quad + i_{qr}(k) \Big(\omega_{pm}(k) L_{mq} - \gamma_{dr} L_{qr} \left(\omega_{pm}(k) - \omega_r(k) \right) \Big) \\ & \quad + i_{qs}(k) \Big(\omega_{pm}(k) L_{qs} - \gamma_{dr} L_{mq} \left(\omega_{pm}(k) \right. \\ & \quad \left. - \omega_r(k) \right) \Big) \Big] \times \frac{T_s}{\sigma_d L_{ds}} + i_{ds}(k) \end{aligned} \tag{18}$$

$$\begin{aligned} & i_{qr}(k+1) \\ & = \Big[V_{qr}^* - \gamma_{qs} V_{qs}^* - r_r i_{qr}(k) + \gamma_{qs} r_s i_{qs}(k) \end{aligned}$$

TABLE 1. Possible switching states and voltage vectors for two-level three-phase inverters shown in Fig. 3.

Switching State (S_1^i, S_2^i, S_3^i)	Synthesized voltage vector	Vector representation
(000)	0	V_{Z1}^i
(100)	$\frac{2}{3}V_{dc}$	V_{A1}^i
(110)	$\frac{1}{3}V_{dc} + j\frac{\sqrt{3}}{3}V_{dc}$	V_{A2}^i
(010)	$-\frac{1}{3}V_{dc} + j\frac{\sqrt{3}}{3}V_{dc}$	V_{A3}^i
(011)	$-\frac{2}{3}V_{dc}$	V_{A4}^i
(001)	$-\frac{1}{3}V_{dc} - j\frac{\sqrt{3}}{3}V_{dc}$	V_{A5}^i
(101)	$\frac{1}{3}V_{dc} - j\frac{\sqrt{3}}{3}V_{dc}$	V_{A6}^i
(111)	0	V_{Z2}^i

$$
\begin{aligned}
&- i_{ds}(k)\Big(\big(\omega_{pm}(k) - \omega_r(k)\big)L_{md} - \gamma_{qs}L_{ds}\omega_{pm}(k)\Big) \\
&- i_{dr}(k)\Big(\big(\omega_{pm}(k) - \omega_r(k)\big)L_{dr} - \gamma_{qs}L_{md}\omega_{pm}(k)\Big) \\
&- \lambda_m\Big(\big(\omega_{pm}(k) - \omega_r(k)\big) - \gamma_{qs}\omega_{pm}(k)\Big)\Big] \times \frac{1}{\sigma_q L_{qr}} \\
&+ i_{qr}(k) \qquad (19)
\end{aligned}
$$

$$
\begin{aligned}
&i_{dr}(k+1) \\
&= \Big[V_{dr}^* - \gamma_{ds}V_{ds}^* - r_r i_{dr}(k) + \gamma_{ds}r_s i_{ds}(k) \\
&+ i_{qs}(k)\Big(\big(\omega_{pm}(k) - \omega_r(k)\big)L_{mq} - \gamma_{ds}L_{qs}\omega_{pm}(k)\Big) \\
&+ i_{qr}(k)\Big(\big(\omega_{pm}(k) - \omega_r(k)\big)L_{qr} \\
&- \gamma_{ds}L_{mq}\omega_{pm}(k)\Big)\Big] \times \frac{T_s}{\sigma_d L_{dr}} + i_{dr}(k) \qquad (20)
\end{aligned}
$$

where T_s is the sampling time. V_s^* and V_r^* are the control variables for stator and rotor windings, respectively. Considering a two-level three-phase inverter for interfacing both stator and inner rotor windings as shown in Fig. 3, the feasible switching states and therefore, the synthesized voltage vectors are summarized in Table 1, where "i" denotes "s" for stator winding and "r" for inner rotor winding. It is worth mentioning that due to employing a FCS-MPC strategy in this paper, the constraints on the control variables are already taken into account. In other words, only valid switching states of the inverters are taken into consideration, which limits the number of switching states to 64.

The objective variables including the electromagnetic torques and linkage fluxes in the next sampling period are then predicted as follows:

$$
\begin{aligned}
T_{e,pm}(k+1) &= \frac{3}{2}p\lambda_m\big(i_{qs}(k+1) + i_{qr}(k+1)\big) \\
T_{e,in}(k+1) &= \frac{3}{2}p\big(\lambda_m i_{qr}(k+1) + \lambda_{ds}(k+1)i_{qr}(k+1) \\
&\quad - \lambda_{qs}(k+1)i_{dr}(k+1)\big) \qquad (21)
\end{aligned}
$$

and

$$
\begin{aligned}
\lambda_{ds}(k+1) &= L_{ds}i_{ds}(k+1) + L_{md}i_{dr}(k+1) + \lambda_m \\
\lambda_{qs}(k+1) &= L_{qs}i_{qs}(k+1) + L_{mq}i_{qr}(k+1) \\
\lambda_{dr}(k+1) &= L_{dr}i_{dr}(k+1) + L_{md}i_{ds}(k+1) + \lambda_m \\
\lambda_{qr}(k+1) &= L_{qr}i_{qr}(k+1) + L_{mq}i_{qs}(k+1) \qquad (22)
\end{aligned}
$$

B. COST FUNCTION

From (17) to (20), it can be deduced that switching states of the stator inverter not only construct the stator voltage, but also have undesirable effects on the inner rotor current and vice versa. This implies that the switching states of the inverters cannot be optimized independently. Therefore, in this paper, a MIMO direct torque MPC is developed, taking into account this undesired electromagnetic interaction between different ports. For this purpose, a common cost function incorporating the error of objective variables from both ports is formulated as follows:

$$
\begin{aligned}
C.F. &= \|T_{e,pm}(k+1) - T_{e,pm}^*\| + w_{pm}\|\lambda_s(k+1) - \lambda_s^*\| \\
&\quad + \|T_{e,in}(k+1) - T_{e,in}^*\| + w_{in}\|\lambda_r(k+1) - \lambda_r^*\| \qquad (23)
\end{aligned}
$$

where $T_{e,pm}^*$ and $T_{e,in}^*$ are the reference torques for the outer and inner rotors, respectively, provided by the speed controllers shown in Fig. 3. λ_s^* and λ_r^* are the reference fluxes for stator and inner rotor, respectively, which are calculated using Eqs. (24) and (25) to guarantee the maximum torque per ampere and minimum losses [8], [14].

$$
\lambda_s^* = \sqrt{\lambda_m^2 + \Big(\frac{L_{sq}}{k}\big(T_{in}^* + T_{pm}^*\big) - \frac{L_{mq}}{k}T_{in}^*\Big)^2} \qquad (24)
$$

$$
\lambda_r^* = \sqrt{\lambda_m^2 + \Big(-\frac{L_{rq}}{k}T_{in}^* + \frac{L_{mq}}{k}\big(T_{in}^* + T_{pm}^*\big)\Big)^2} \qquad (25)
$$

where $k = \sqrt{3/2} \times p \times \lambda_m$. It is noted that to balance the cost function, all variables involved in the function have been normalized. The weighting factor, w_{pm} and w_{in}, are then used for prioritizing between torque and flux errors. In a conventional MPC [24], the weighing factor is defined as $w = T_n/\lambda_n$ to give the same precedence to both objectives. In the proposed strategy, however, the normalized values are used for torque and flux components incorporated in the cost function. Therefore, the weighing factors are set to 1 to balance the objectives in the cost function. Furthermore, in order to demonstrate that setting the weighting factors equal to 1 yields the optimal results, the tracking error of the control objectives provided in Eq. (23) is measured, while varying the weighting factors between 0.1 and 1. As shown in Fig. 4, the minimum error is obtained when both weighting factors are set to 1.

C. VALID SWITCHING STATES

To account for the interaction between ports, all feasible switching states of the two inverters should be simultaneously considered. In other words, rather than optimizing the switching state of each inverter independently by evaluating its individual cost function with eight valid switching vectors, the two inverters are virtually combined to form a six-leg converter. As a result, there are now 2^6 valid switching states that need to be considered at each sampling time to determine the best switching state for both ports concurrently. According to (17) and (18), the stator current depends on the voltage vectors created by both stator and inner rotor

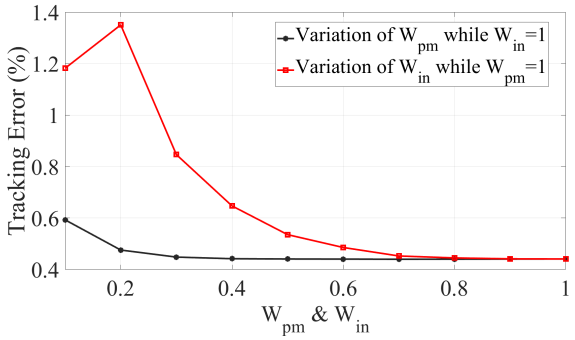

FIGURE 4. Variation of tracking error versus the variation of weighting factors.

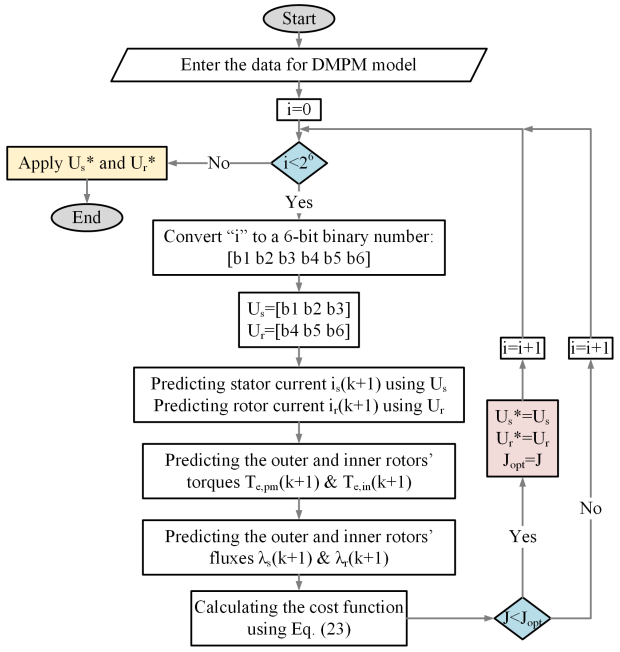

FIGURE 5. The procedure of finding the optimum switching states of the inverters during each sampling period.

inverters, while only the switching states of the stator-side inverter are considered to predict the stator current in the SISO-based strategy. On the other hand, the inner rotor current also depends on the voltage vectors created by both electric ports (see (19)-(20)), but the SISO-based strategy only evaluates the switching states of the inner rotor inverter to predict the inner rotor current and optimize the switching state. In the proposed strategy, the DMPM is considered as MIMO system in which the switching states of both ports are optimized simultaneously considering the mutual effects between the switching states of different ports. As a result, the undesired electromagnetic interactions caused by individual control of different ports can be mitigated by the proposed strategy.

The procedure for finding the optimum switching state at each sampling time is depicted in Fig. 5. As can be seen, the DMPM's parameters are first given to the controller. By defining the counter i, a decimal value corresponding to each possible switching state is created in every iteration. This decimal value is then converted to a 6-bit binary number, which represents the i-th switching vector candidate. The three most significant bits and the three least significant bits of the binary number are respectively considered the i-th switching vectors of the stator and inner rotor windings. The stator and inner rotor currents are then predicted using Eqs. (17) to (20) considering the generated candidate switching states. The torques and fluxes for both ports are also calculated using Eqs. (21) and (22). Finally, the cost function defined in (23) is calculated for the corresponding candidate switching vector, and it is selected as the optimum one if it leads to the minimum cost function. Otherwise, it is not considered, and by increasing the counter, the next possible switching vector is produced and the calculation repeats.

TABLE 2. Specification of dual mechanical port machine.

Parameter	λ_m	r_r	r_s	L_{dr}	L_{qr}	L_{ds}
Unit	Wb	Ω	Ω	mH	mH	mH
Value	0.2	0.2	0.35	3	4.5	9
Parameter	L_{qs}	L_{md}	L_{mq}	Pole pairs	J_{out}	J_{in}
Unit	mH	mH	mH	-	kg/m^2	kg/m^2
Value	15	0.5	1.5	2	0.1	0.16

IV. SIMULATION RESULTS

The performance of the proposed MPDTC strategy is evaluated under different operating conditions. For this purpose, different speed and load torque profiles are considered as shown in Fig. 6. Despite the fact that the inner rotor only functions as a generator in a HEV due to its direct connection to internal combustion engine, as shown in Fig. 1, the load applied to the inner rotor contains both positive and negative values to confirm the performance of the proposed MPDTC in four-quadrant operation. The specification of the DMPM is summarized in Table 2. Figs. 6(a) and (b) illustrate the rotational speeds of the outer and inner rotors when the conventional PI controller is used, where PI controllers are tuned using the Ziegler–Nichols method. As can be seen, the speed of the outer rotor is inversely affected by the speed and torque variations of the inner rotor. The green circles and squares show the moment when the torque and speed of the inner rotor change, respectively. As depicted in Fig. 6(c) the electromagnetic torque in the outer rotor is considerably affected by torque variations in the inner rotor, confirming the unfavorable interactions between ports. It can also be deduced from Fig. 6(c) and (d) that the electromagnetic torques suffer from a significant ripple of around 40%.

Considering the same operating conditions, the performance of the DMPM controlled by a SISO based model predictive current control is evaluated as presented in Fig. 7. Despite experiencing improvements in terms of torque ripple (see Fig. 7(c) and (d)) and transient response (see Fig. 7(a) and (b)) compared with the conventional PI controller, the DMPM still encounters undesired electromagnetic interactions between ports that have an adverse impact on the independent control of the mechanical ports. Using the

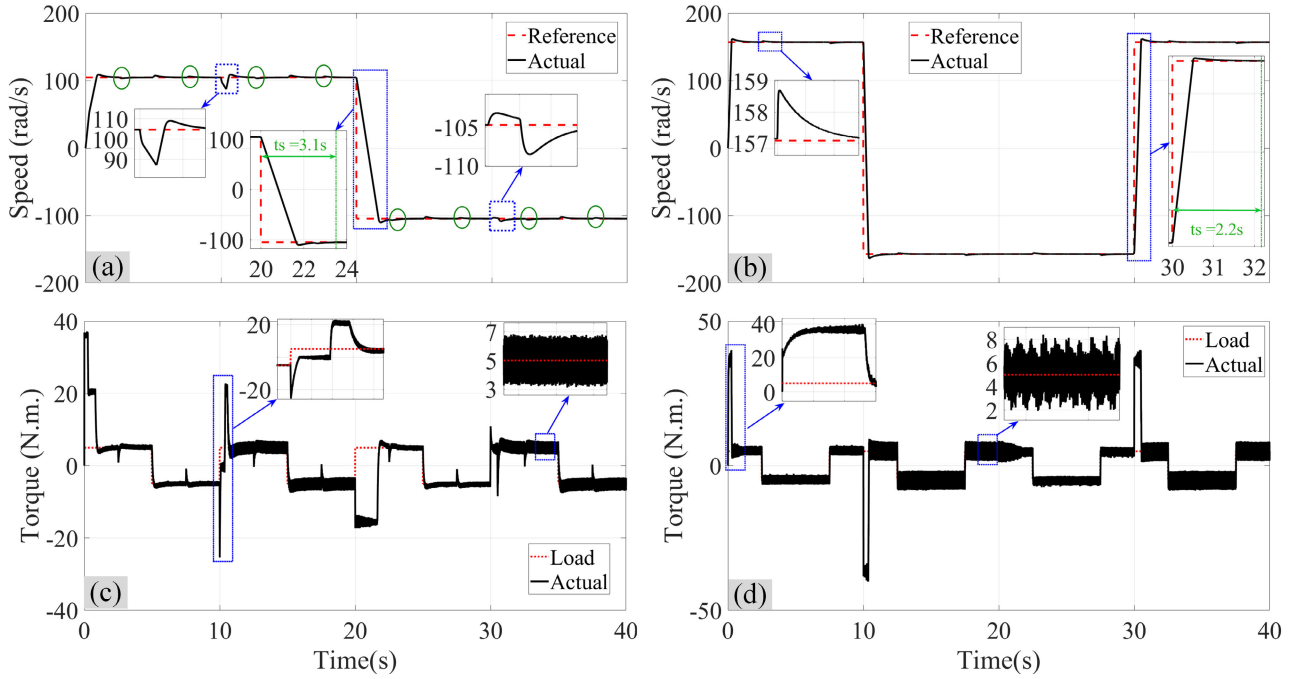

FIGURE 6. Simulations results with conventional FOC control, (a) rotational speed of the outer rotor, (b) rotational speed of inner rotor, (c) electromagnetic torque of the outer rotor, and (d) electromagnetic torque of the inner rotor.

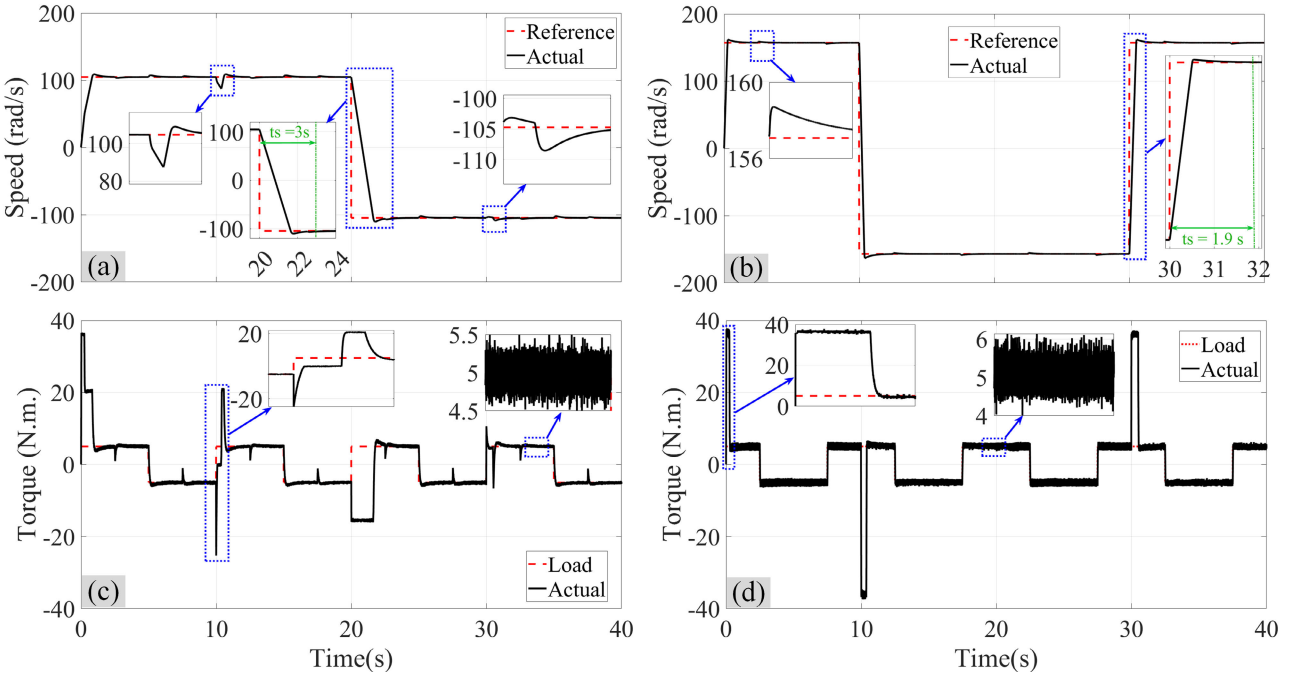

FIGURE 7. Simulations results with SISO based model predictive current control strategy, (a) rotational speed of the outer rotor, (b) rotational speed of inner rotor, (c) electromagnetic torque of the outer rotor, and (d) electromagnetic torque of the inner rotor.

same reference speed and torque profiles, the simulation results when the proposed MPDTC is utilized are presented in Fig. 8. As shown in Figs. 8(c) and (d), there is no undesired effect on the outer rotor caused by inner rotor torque variations, indicating that the proposed strategy can effectively mitigate the undesired flux interaction between the ports. This results in precise speed control of the inner and outer rotors, as depicted in Figs. 8(a) and (b), respectively. Compared with the PI control strategy, the proposed approach also improves the dynamic performance of the machine in terms of settling time and torque ripple. In Fig. 8(d), the moments at 10 seconds and 30 seconds correspond to significant changes in the direction of the inner rotor's rotational speed. At 10 seconds, the speed reference shifts

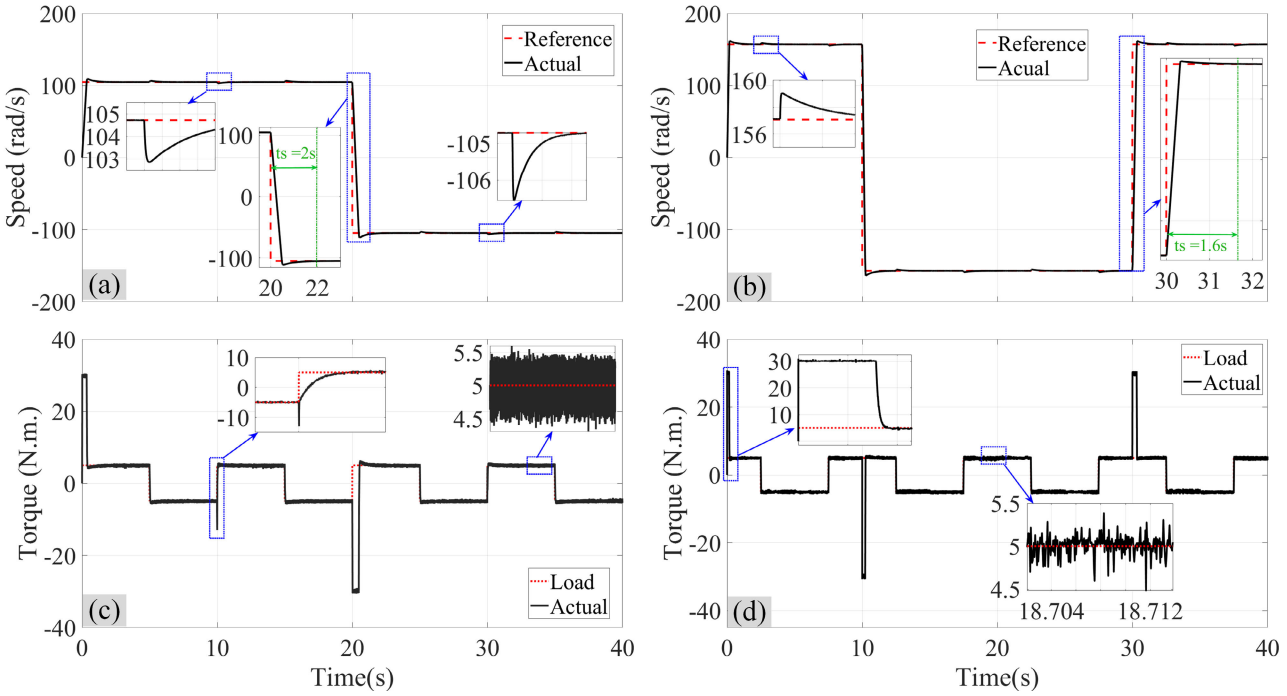

FIGURE 8. Simulations results with proposed MIMO model predictive direct control strategy, (a) rotational speed of the outer rotor, (b) rotational speed of inner rotor, (c) electromagnetic torque of the outer rotor, and (d) electromagnetic torque of the inner rotor.

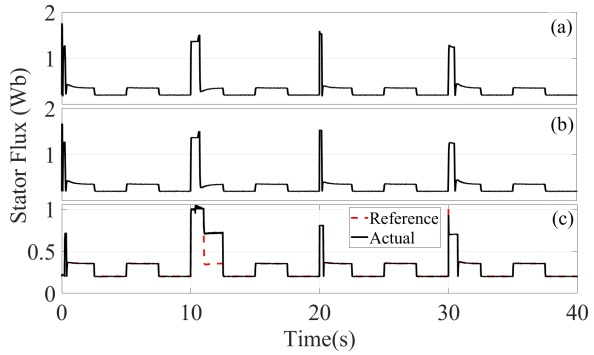

FIGURE 9. Stator linkage flux, (a) conventional FOC strategy, (b) SISO-based MPC, and (c) proposed MPDTC strategy.

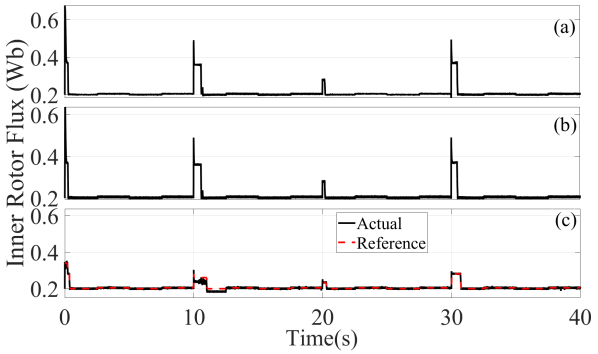

FIGURE 10. Inner rotor linkage flux, (a) conventional FOC strategy, (b) SISO-based MPC, and (c) proposed MPDTC strategy.

from 157 rad/s to -157 rad/s. Consequently, while a positive load is applied to the inner rotor, a substantial negative electromagnetic torque is required to decelerate the rotational speed from 157 rad/s to 0 rad/s, and subsequently accelerate it in the opposite direction to reach -157 rad/s. Similarly, at 30 seconds, the speed reference changes from -157 rad/s to 157 rad/s, demanding a high positive electromagnetic torque to decelerate the speed from -157 rad/s to 0 rad/s, and then accelerate it in the opposite direction.

The proposed strategy can precisely track the reference values for stator and inner rotor fluxes, as shown in Figs. 9 and 10, respectively. Three-phase stator and inner rotor current in presence of different control strategies are respectively demonstrated in Figs. 11 and 12. As can be seen, the variations of the current are well-matched with the variations of the load torques. The zoomed out intervals demonstrate the moment that the rotational speed of the rotors reverse. As a result, the frequency of the currents reduce and their polarity change.

To highlight the superior dynamic performance of the proposed strategy compared with the conventional methods, a quantitative comparison is provided in Table 3 in which the settling time and overshoot of the outer rotor are considered as comparison criteria. As can be seen, the proposed strategy not only offers an undesired electromagnetic interaction cancellation capability, but it also improves the dynamic response of the DMPM in terms of settling time and overshoot.

V. HARDWARE-IN-THE-LOOP RESULTS

To validate the proposed MPDTC strategy, its performance for independent speed control of inner and outer rotors is evaluated using hardware-in-the-loop (HIL) results. To this

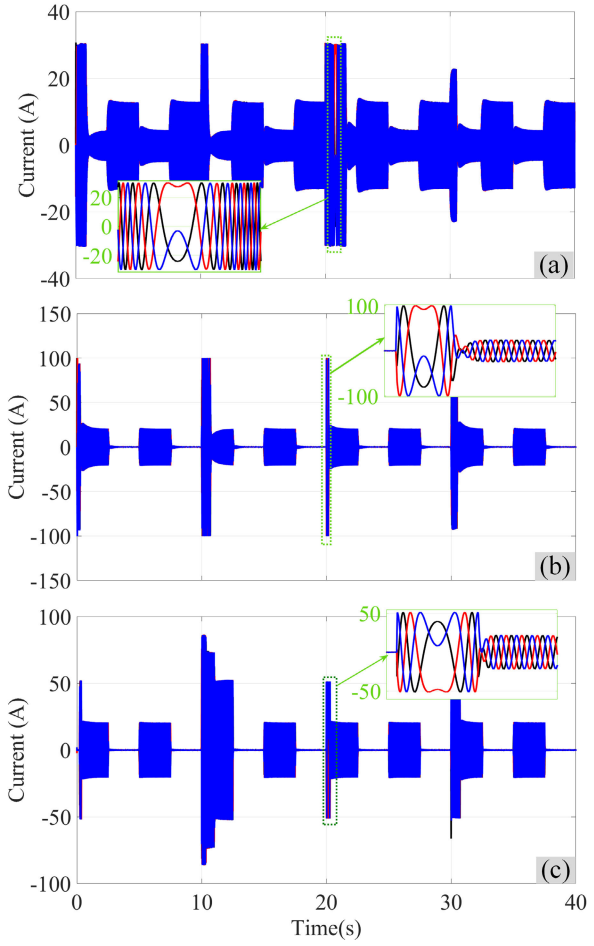

FIGURE 11. Three-phase current of the stator winding, (a) conventional FOC strategy, (b) SISO-based MPC, and (c) proposed MPDTC.

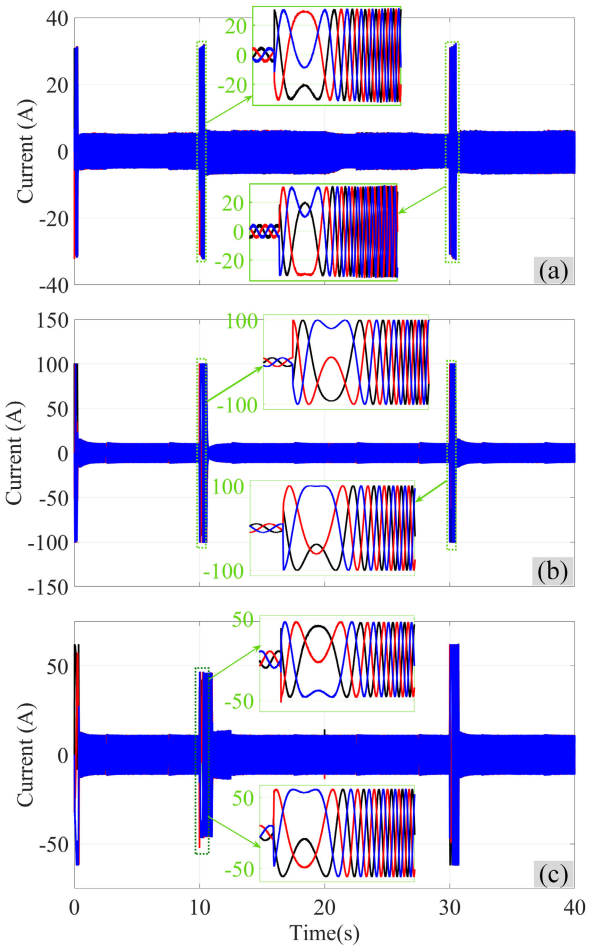

FIGURE 12. Three-phase current of the inner rotor winding, (a) conventional FOC strategy, (b) SISO-based MPC strategy, and (c) proposed MPDTC strategy.

end, Typhoon HIL 602 and dSPACE 1103 are respectively used to implement the electrical parts, including inverters and DMPM, and the control part in real-time. The HIL test setup is shown in Fig. 13. Fig. 14 depicts the rotational speed of inner and outer rotors when the applied loads are changed in a constant reference speed while using the conventional FOC and proposed MTDPC. As expected, the variations in the inner rotor speed affects the outer rotor speed, confirming the undesired electromagnetic interaction between ports in the conventional control strategy. However, when the proposed MPDTC is applied, this electromagnetic interaction is removed, so that the load changes in the inner rotor do not affect the rotational speed of the outer rotor. The performance of the DMPM in tracking a speed change for inner and outer rotors in presence of conventional and proposed MPDTC is compared in Fig. 15. Again, it is revealed that the proposed strategy successfully mitigates the undesired electromagnetic coupling between inner and outer rotors, such that the inner rotor's speed is not affected by the speed change of the inner rotor. It can be also deduced from Fig. 15 that the proposed MPDTC can improve the dynamic performance of the DMPM compared to the conventional FOC strategy. Three-phase currents for stator and inner rotor

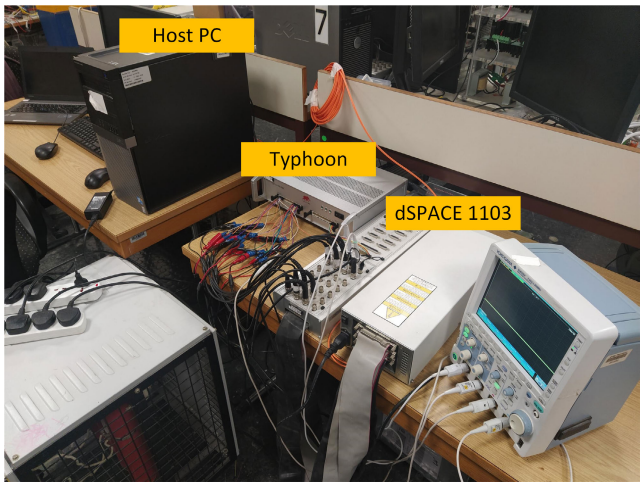

FIGURE 13. Hardware-in-the-loop setup.

windings in presence of MPDTC strategy are also illustrated in Fig. 16. The quantitative comparison of the HIL results is summarized in Table 4. It is successfully revealed that the proposed strategy can significantly improve the dynamic performance of the DMPM compared with the conventional

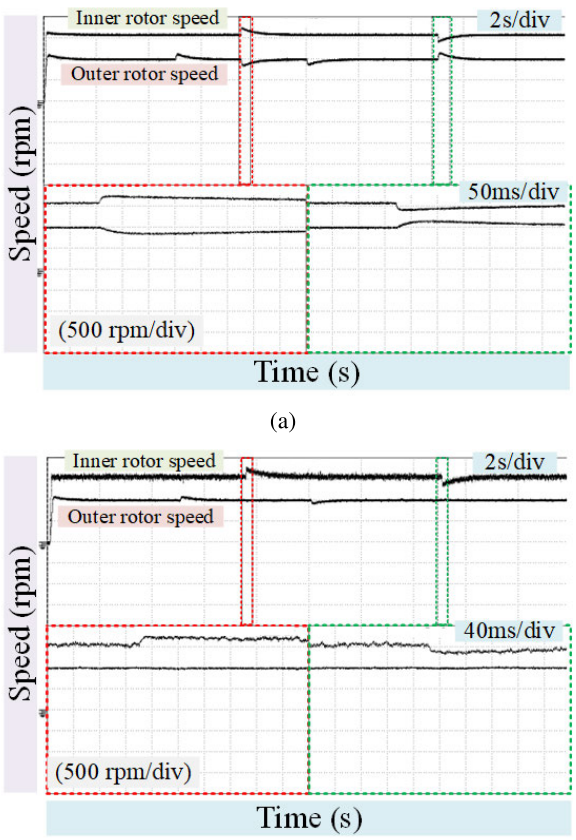

FIGURE 14. HIL results - rotational speed of inner and outer rotors, (a) conventional FOC strategy, and (b) proposed MPDTC strategy.

TABLE 3. Quantitative comparison of simulation results.

Comparison Criteria	PI-based FOC	SISO-based MPC	Proposed Strategy
Settling time (s)	3.1	3	2
Overshoot (%)	4.1	4.05	4.02
Interaction Cancellation	×	×	✓

FOC control strategy. In terms of output ripple, however, the proposed strategy stands in the second rank.

It is noted that the FS-MPC strategy employed in this study falls under the category of constant state per sample (CSPS) control techniques, wherein the switching state remains unchanged during each sampling period. As a consequence, if the output deviates beyond the expected upper or lower band around the reference value, the control signal remains unaltered, potentially resulting in a higher-than-anticipated output ripple. In contrast, the conventional PWM control strategy allows for modulation of the switching pulse within each switching period, enabling fine control over the output ripple. To address the issue of higher ripple encountered in CSPS control strategies, an increase in the sampling frequency may prove beneficial. By elevating the sampling frequency, the system can more swiftly adapt to variations in the output, reducing the magnitude of ripple and enhancing the overall control performance. However, achieving a higher sampling frequency to reduce the ripple

TABLE 4. Quantitative Comparison of the HIL Results.

Comparison Criteria	PI-based FOC	Proposed Strategy
Settling time (s)	2.5	1.8
Overshoot (%)	30	19
Speed ripple	Low	High
Interaction Cancellation	×	✓

in the proposed strategy presents challenges in real-time implementation. As a result, the proposed strategy may exhibit a higher output ripple, as demonstrated in Fig. 14 and Fig. 15. In Section III-C, it is elucidated that the computational burden of the proposed strategy is amplified due to an increased number of possible switching states to be evaluated in each sampling interval-rising from 16 in the conventional SISO-based MPC to 64 in the proposed strategy. Consequently, the processor necessitates additional processing time to assess all the switching candidates while simultaneously avoiding any overruns in real-time applications. To sum up, while a higher sampling frequency may theoretically mitigate ripples in the proposed strategy, it becomes impractical to implement in real-time due to the increased computational requirements. Balancing the trade-off between control accuracy and real-time feasibility remains a critical consideration when deploying the proposed FS-MPC strategy in practical applications.

VI. REAL-TIME EXECUTION ANALYSIS

Compared with the SISO-based MPC strategy, where the switching states of each inverter are evaluated separately, the computational burden of the proposed strategy is relatively higher. In the classical approach, 16 switching states need to be evaluated in each sampling time, while in the proposed strategy, there are 64 switching states to be evaluated to find the optimum control action for the next sampling instant. However, it can be deduced from the hardware-in-the loop results that the proposed strategy can be executed in real-time. Additionally, the computation time can be roughly calculated to verify the execution time of the proposed strategy. As shown in Figure 5, the stator and inner rotor currents are initially predicted using Eqs. (20)-(17) for each possible switching state. Then, the electromagnetic torques and fluxes are calculated by Eqs. (21)-(22). Finally, the cost function for the corresponding switching state is obtained using Eq. (23). In total, 120 × 64 multiplication, 66 × 64 addition, and 64 comparison operations (where 64 is the number of possible switching states) should be executed in each sampling time. Referring to the datasheet of the TMS320F28379D microcontroller (as an example) with a clock cycle of 200 MHz, it can be understood that this commercial microcontroller is able to execute 200 million instructions per second [25]. This means that the microcontroller at least needs 60 μs to execute the proposed strategy in real-time. Assuming a sampling time of 100 μs (to have a maximum switching frequency of 10 kHz in the FS-MPC strategy), it is therefore verified that the proposed strategy can be executed in real-time without any overrun.

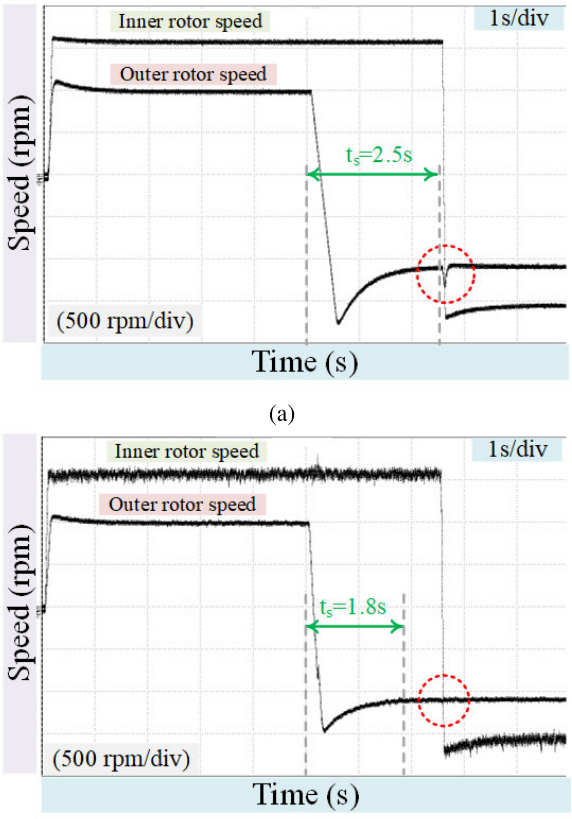

FIGURE 15. HIL results - rotational speed of inner and outer rotors, (a) conventional FOC strategy, and (b) proposed MPDTC strategy.

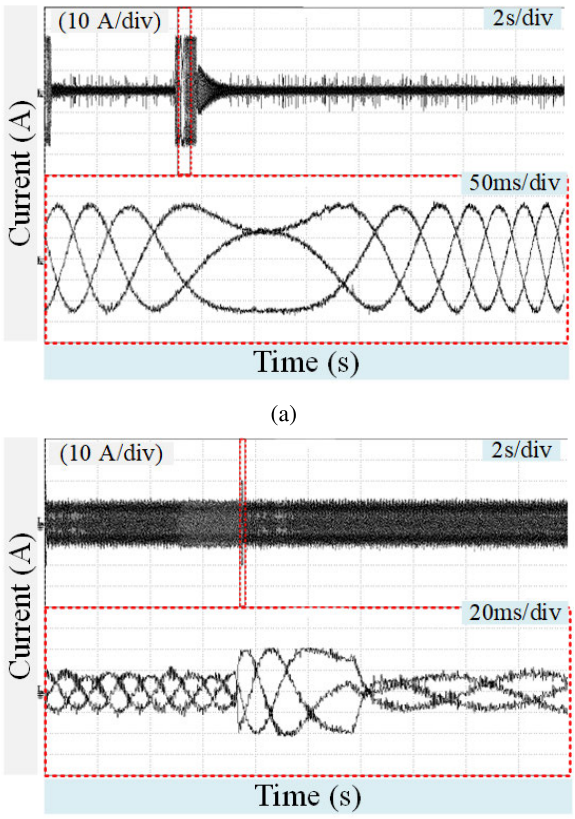

FIGURE 16. HIL results in presence of proposed MPDTC strategy, (a) stator's three-phase currents, and (b) inner rotor's three-phase currents.

TABLE 5. Quantitative comparison between computational burden of SISO-based and MIMO-based strategies.

Control Strategy	SISO-based MPC	Proposed Strategy
Number of Multiplication	120×16	120×64
Number of addition	66×16	66×64
Number of Comparison	16	65
Minimum Execution Time (μs)	20	60

The comparison between the computational effort of the proposed strategy and the conventional SISO-based MPC is provided in Table 5. As stated earlier, the proposed strategy leads to enhanced dynamic performance in exchange for high computational burden compared with the conventional method. However, this higher calculation time does not cause any overrun and/or data loss in real-time implementation, as verified by HIL results.

VII. SENSITIVITY ANALYSIS

It is obvious that the proposed predictive control is a model-based strategy, and therefore, its performance might be affected if there is an error between the parameters used in the controller and the ones used in the laboratory setup. To evaluate this effect, a sensitivity analysis is provided in this section. For this purpose, the stator parameters (r_s and L_s), rotor parameters (r_r and L_r), and mutual inductance (L_m) are varied from 50% and 150% of their nominal value once a time in the predictive model given in (17) to (22). In this analysis, the nominal parameters are named r_{s0}, L_{s0}, r_{r0}, L_{r0}, and L_{m0} while the variations in the parameters are defined as $\Delta R_s = r_s/r_{s0}$, $\Delta R_r = r_r/r_{r0}$, $\Delta L_s = L_s/L_{s0}$, $\Delta L_r = L_r/L_{r0}$, and $\Delta L_m = L_m/L_{m0}$. According to [9], an DMPM based HEV can operate in five operating modes: i.e., a) start-up, b) normal, c) acceleration, d) recharging, and e) braking. In start-up mode, the battery is responsible for providing the requested power by HEV. Therefore, while the requested power by HEV (P_{HEV}) is positive ($\omega_{HEV} > 0$ & $T_{HEV} > 0$), the power provided by ICE (P_{ICE}) sets to zero ($\omega_{ICE} = 0$ & $T_{ICE} = 0$) for keeping its efficiency within the optimum region. In normal mode, the requested power by HEV can be completely provided by ICE, meaning that $P_{HEV} = P_{ICE}$. Depending on the speed and torque, two conditions can take place in this mode. In the first condition, $\omega_{ICE} > \omega_{HEV}$ while $T_{ICE} < T_{HEV}$. In the second one, however, $\omega_{ICE} < \omega_{HEV}$ and $T_{ICE} > T_{HEV}$. In acceleration mode, the requested power by HEV is greater than the provided power by ICE ($P_{HEV} > P_{ICE}$). Therefore, both the battery and the ICE jointly provide the required power. In re-charging mode, the generated power by ICE is greater than the requested power by HEV ($P_{HEV} < P_{ICE}$) so that the surplus power can be used to re-charge the battery. Finally, in the braking mode, the requested power by HEV is negative ($\omega_{HEV} > 0$

TABLE 6. Different test conditions used for sensitivity analysis of the proposed strategy.

Test Number	Operating mode	PM rotor parameters			Inner rotor parameters		
		P_{ICE} (W)	ω_{ICE} (rad/s)	T_{ICE} (N.m.)	P_{HEV} (W)	ω_{HEV} (rad/s)	T_{HEV} (N.m.)
1	Start-up	0	0	0	5000	500	10
2	Normal	5000	1000	5	5000	500	10
3		5000	500	10	5000	1000	5
4	Acceleration	5000	1000	5	10000	1000	10
5	Recharge	10000	1000	10	5000	500	10
6	Braking	0	0	0	-5000	500	-10

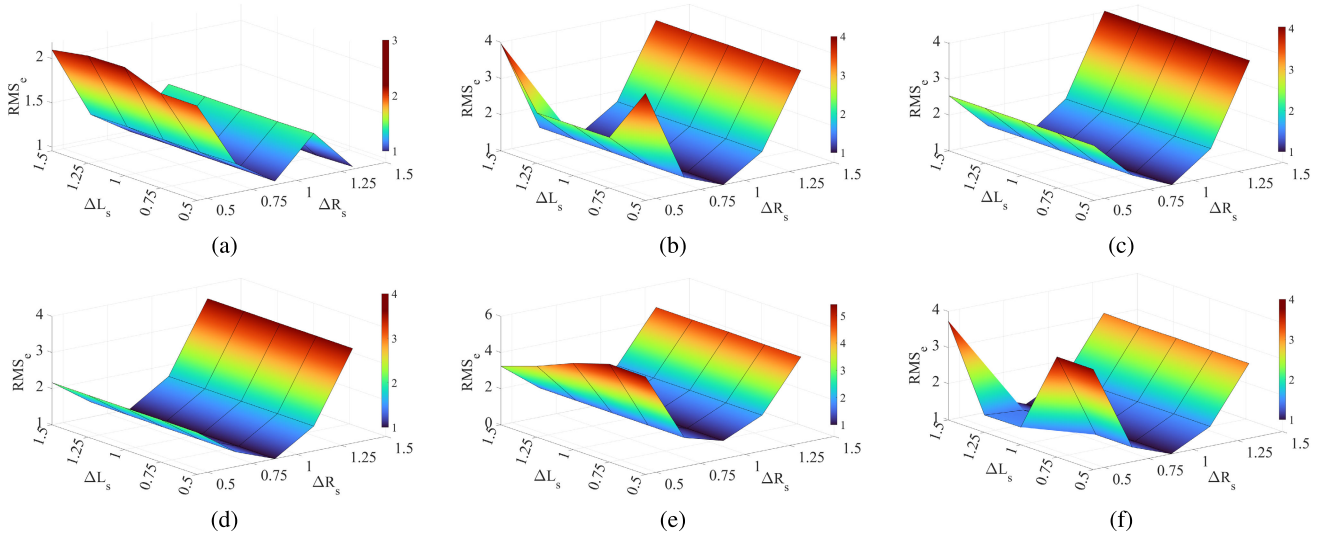

FIGURE 17. Sensitivity results of the proposed strategy to simultaneous variations of r_s and L_s, (a) Test 1, (b) Test 2, (c) Test 3, (d) Test 4, (e) Test 5, and (f) Test 6.

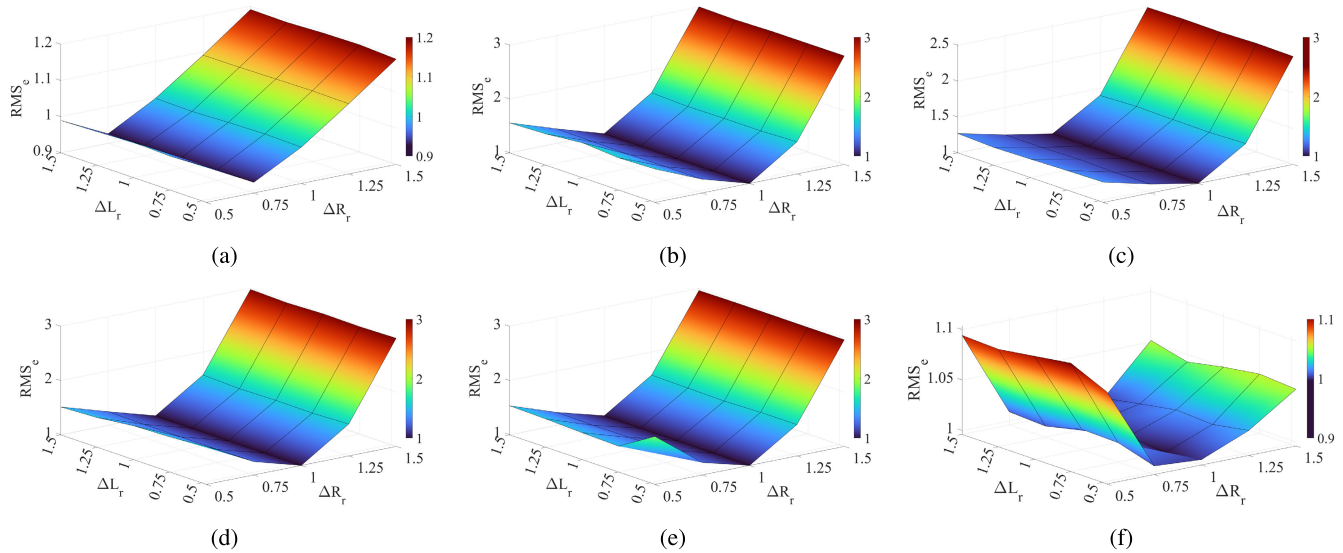

FIGURE 18. Sensitivity results of the proposed strategy to simultaneous variations of r_r and L_r, (a) Test 1, (b) Test 2, (c) Test 3, (d) Test 4, (e) Test 5, and (f) Test 6.

& $T_{HEV} < 0$) while the power provided by ICE is zero ($\omega_{ICE} = 0$ & $T_{ICE} = 0$). To cover all operating modes, the test conditions summarized in Table 6 are considered to evaluate the sensitivity of the proposed strategy.

Root-Mean-Square error (RMSe) between the reference values of the control objectives ($T_{e,pm}$, $T_{e,in}$, λ_s, and λ_r) and their measured values, as expressed by (26), is utilized as the evaluation criterion.

$$RMS_e = \frac{1}{4}\sum_{m=1}^{4}\sqrt{\frac{1}{N}\sum_{j=1}^{N}(f^*(j) - f(j))^2} \tag{26}$$

where N is the number of samples taken during the simulation so that the control errors in both transient and steady-state

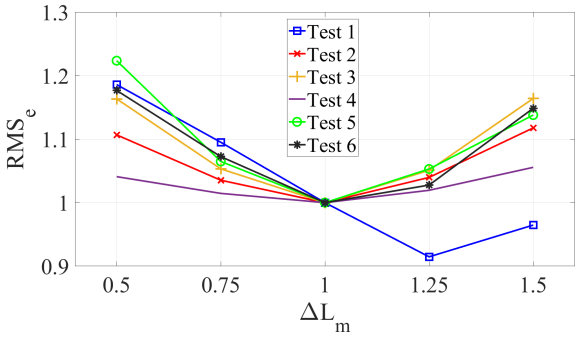

FIGURE 19. Sensitivity analysis results of the proposed strategy to the variation of mutual inductance (L_m).

modes are considered. f also represents the variables whose error values are calculated. It is worth mentioning that the normalized values of the torque and flux are considered for calculating RMSe to make it unit-less and more comparable.

The impact of variations in stator parameters are shown in Fig. 17. As can be seen, the variations in the stator's inductance do not have a significant effect on the performance of the proposed strategy under all operating conditions. However, the functionality of the MPDTC can be inversely affected in presence of stator's resistance values different from the nominal one. Figure 18 depicts the effect of variations in the inner rotor's parameters under different operating conditions. It is deduced that the performance of the proposed MTDTC strategy is almost independent from inner rotor's inductance. However, its precise performance is highly dependent on the inner rotor's resistance, where inaccuracies in the inner rotor's resistance lead to a decrease in the accuracy of the proposed control strategy. The influence of the mutual inductance mismatch on the performance of the proposed strategy is illustrated in Fig. 19. As can be seen, the accuracy of the proposed control strategy is slightly affected in the presence of the mismatch in mutual inductance. Whereas the robustness of the proposed strategy against parameter uncertainties is verified using the sensitivity analysis, it is worth to incorporate an anti-parameter disturbance technique into the proposed strategy to assure the precise control in a wide operating range.

VIII. CONCLUSION

In this paper, a novel multi-input multi-output based model predictive direct torque control strategy was developed to reduce the undesired electromagnetic coupling between the mechanical ports of a dual mechanical port machine. By utilizing the discretized dynamic equations of the machine, a MIMO cost function was defined to consider both torque and flux errors in both ports. Unlike traditional approaches that optimize the switching states of each inverter independently, the proposed MPDTC merges the switching states of both inverters to take into account the interaction between the mechanical ports.

Simulation and experimental results showed that the proposed MPDTC was able to minimize the coupling between the ports and prevent the load and speed variations in one port from affecting the speed of the other port. The effectiveness of the MPDTC is confirmed through hardware-in-the-loop experiments using Typhoon HIL 602 and dSPACE 1103. The results demonstrated that the proposed strategy successfully eliminated the undesired coupling effects between the mechanical ports without causing a heavy computational burden.

A sensitivity analysis was conducted, and it was found that the performance of the MPDTC was not significantly impacted by changes in the stator and inner rotor resistances. However, excessive variations in the inductance values of the stator and inner rotor windings could affect the accuracy of the MPDTC.

REFERENCES

[1] L. Xu, "Dual-mechanical-port electric machines-concept and application of a new electric," *IEEE Ind. Appl. Mag.*, vol. 15, no. 4, pp. 44–51, Jul. 2009.
[2] X. Ren, D. Li, R. Qu, X. Han, and Z. Liang, "A brushless dual-electrical-port dual-mechanical-port machine with integrated winding configuration," *IEEE Trans. Ind. Electron.*, vol. 68, no. 4, pp. 3022–3032, Apr. 2021.
[3] C. Li, X. Guo, J. Fu, W. Fu, Y. Liu, H. Chen, R. Wang, and Z. Li, "Design and analysis of a novel double-stator double-rotor motor drive system for in-wheel direct drive of electric vehicles," *Machines*, vol. 10, no. 1, p. 27, Dec. 2021.
[4] C. U. Ubadigha and M.-C. Tsai, "Analysis of integrated magnetic gear motor with dual mechanical output port: A block diagram approach," *IEEE Trans. Energy Convers.*, vol. 35, no. 3, pp. 1301–1308, Sep. 2020.
[5] A. Dalal and P. Kumar, "Design, prototyping, and testing of a dual-rotor motor for electric vehicle application," *IEEE Trans. Ind. Electron.*, vol. 65, no. 9, pp. 7185–7192, Sep. 2018.
[6] L. Xu, Y. Zhang, and X. Wen, "Multioperational modes and control strategies of dual-mechanical-port machine for hybrid electrical vehicles," *IEEE Trans. Ind. Appl.*, vol. 45, no. 2, pp. 747–755, Mar./Apr. 2009.
[7] A. Ghayebloo and A. Radan, "Superiority of dual-mechanical-port-machine-based structure for series–parallel hybrid electric vehicle applications," *IEEE Trans. Veh. Technol.*, vol. 65, no. 2, pp. 589–602, Feb. 2016.
[8] M. Ghanaatian and A. Radan, "Application and simulation of dual-mechanical-port machine in hybrid electric vehicles," *Int. Trans. Electr. Energy Syst.*, vol. 25, no. 6, pp. 1083–1099, Jun. 2015.
[9] H. Bizhani, G. Yao, S. M. Muyeen, S. M. Islam, and L. Ben-Brahim, "Dual mechanical port machine based hybrid electric vehicle using reduced switch converters," *IEEE Access*, vol. 7, pp. 33665–33676, 2019.
[10] X. Sun, M. Cheng, W. Hua, and L. Xu, "Optimal design of double-layer permanent magnet dual mechanical port machine for wind power application," *IEEE Trans. Magn.*, vol. 45, no. 10, pp. 4613–4616, Oct. 2009.
[11] X. Sun and M. Cheng, "Thermal analysis and cooling system design of dual mechanical port machine for wind power application," *IEEE Trans. Ind. Electron.*, vol. 60, no. 5, pp. 1724–1733, May 2013.
[12] W. Ullah, F. Khan, and S. Hussain, "A comparative study of dual stator with novel dual rotor permanent magnet flux switching generator for counter rotating wind turbine applications," *IEEE Access*, vol. 10, pp. 8243–8261, 2022.
[13] N. Baloch, J.-W. Kwon, M. Ayub, and B.-I. Kwon, "Low-cost dual-mechanical-port dual-excitation machine for washing machine application," *IEEE Access*, vol. 7, pp. 87141–87149, 2019.
[14] A. Flah, I. A. Khan, A. Agarwal, L. Sbita, and M. G. Simoes, "Field-oriented control strategy for double-stator single-rotor and double-rotor single-stator permanent magnet machine: Design and operation," *Comput. Electr. Eng.*, vol. 90, Mar. 2021, Art. no. 106953.
[15] J. Druant, H. Vansompel, F. De Belie, and P. Sergeant, "Optimal control for a hybrid excited dual mechanical port electric machine," *IEEE Trans. Energy Convers.*, vol. 32, no. 2, pp. 599–607, Jun. 2017.
[16] H. Cai and L. Xu, "Modeling and control for cage rotor dual mechanical port electric machine—Part II: Independent control of two rotors," *IEEE Trans. Energy Convers.*, vol. 30, no. 3, pp. 966–973, Sep. 2015.

[17] Z. Njajra, A. Flah, D. E. Chariag, and L. Sbita, "A PMDRM decoupling vector control strategy for EVT drive in hybrid vehicles," in *Proc. Int. Conf. Green Energy Convers. Syst. (GECS)*, Mar. 2017, pp. 1–6.
[18] X. Han, W. Kong, R. Qu, D. Li, T. Zou, X. Ren, T. Pei, K. Yang, and C. Gan, "Flexible energy conversion control strategy for brushless dual-mechanical-port dual-electrical-port machine in hybrid vehicles," *IEEE Trans. Power Electron.*, vol. 34, no. 4, pp. 3910–3920, Apr. 2019.
[19] M. F. Elmorshedy, W. Xu, F. F. M. El-Sousy, M. R. Islam, and A. A. Ahmed, "Recent achievements in model predictive control techniques for industrial motor: A comprehensive state-of-the-art," *IEEE Access*, vol. 9, pp. 58170–58191, 2021.
[20] Z. Njajra, A. Flah, D. E. Chariag, and L. Sbita, "Model predictive controller application to a dual rotor motor," in *Proc. Int. Conf. Green Energy Convers. Syst. (GECS)*, Mar. 2017, pp. 1–6.
[21] H. Wu, W. Zhao, M. Yu, and X. Wang, "Design and simulation of a model predictive control system for a novel dual-rotor flux-switching permanent magnet motor," in *Proc. IEEE Int. Conf. Predictive Control Electr. Drives Power Electron. (PRECEDE)*, Nov. 2021, pp. 382–386.
[22] L. Cao, Y. Zhou, G. Yang, Y. He, S. Xie, and C. H. T. Lee, "Decoupling analysis of brushless dual-mechanical-port dual-electrical-port machines," *IEEE Trans. Ind. Electron.*, pp. 1–13, 2023.
[23] Q. Lin, S. Niu, F. Cai, W. Fu, and L. Shang, "Design and optimization of a novel dual-PM machine for electric vehicle applications," *IEEE Trans. Veh. Technol.*, vol. 69, no. 12, pp. 14391–14400, Dec. 2020.
[24] M. G. Farajzadeh Devin, S. K. Hosseini Sani, and H. Bizhani, "Dynamic performance improvement of induction motors used in rolling mill application: A two-loop model predictive control strategy," *ISA Trans.*, vol. 140, pp. 134–143, Sep. 2023.
[25] K. W. Schachter, "TMS320F2837xD microcontroller workshop," in *Workshop Guide Lab Manual*. Sugar Land, TX, USA: Texas Instruments, 2018.

HAMED BIZHANI (Member, IEEE) was born in Mashhad, Iran, in 1988. He received the B.Sc. degree in electrical engineering from Birjand University, Birjand, Iran, in 2011, the M.Sc. degree in electrical engineering from the K. N. Toosi University of Technology, Tehran, Iran, in 2013, and the Ph.D. degree in electrical engineering from the University of Zanjan, in 2019. He was a Visiting Research Associate with Curtin University, Perth, Australia, in 2017. He is currently a Research Assistant with Qatar University, Doha, Qatar. His current research interests include multi-port power electronic converters, control and integration of distributed generations, space vector modulation, model predictive control, and hybrid electric vehicles.

LAZHAR BEN-BRAHIM (Life Senior Member, IEEE) received the B.Sc. and M.Sc. degrees in electrical engineering from the National School of Engineers of Tunis, Tunisia, in 1985 and 1987, respectively, and the Ph.D. degree in electrical engineering from Yokohama National University, Yokohama, Japan, in 1991. From 1991 to 1997, he was with Toshiba Corporation, where he was engaged in the research and development of power electronics and motor drive systems. Since September 1997, he has been with the Industrial Technology Department, College of Technology, Qatar University. He was the Head of the Industrial Technology Department, from 1998 to 2005. In September 2005, he joined the Electrical Engineering Department, Qatar University. He was the Industrial Electronics Chair of RasGas (QatarGas) Company and the Head of the Electrical Engineering Department. He invented several new techniques for use in motor drives, power electronics, sensors, and related areas. These inventions are registered in more than 12 international patents. His current research interests include power electronics, renewable energy, electric vehicles, electric drives, and sensor and instrumentation. He was an Associate Editor of the *Electrical Engineering* (Springer). He is an Editor of the *Electronics* (MDPI).

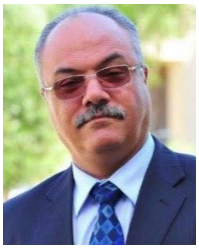

ADEL GASTLI (Senior Member, IEEE) received the B.Sc. degree in electrical engineering from the National School of Engineers of Tunis, Tunisia, in 1985, and the M.Sc. and Ph.D. degrees in electrical and computer engineering from the Nagoya Institute of Technology, Japan, in March 1990 and March 1993, respectively. From September 1985 to September 1987, he was with the National Institute for Standards and Intellectual Property, Tunisia. He was with Mitsubishi Electric Corporation, Japan, from April 1993 to July 1995. He joined the Electrical and Computer Engineering Department, Sultan Qaboos University, Oman, in August 1995. He was the Head of the Department, from September 2001 to August 2003 and from September 2007 to August 2009. He was the Director of the Quality Assurance Office, Sultan Qaboos University, from February 2010 to January 2013. In February 2013, he joined the Electrical Engineering Department, Qatar University, as a Professor and the Kahramaa-Siemens Chair of energy efficiency. From August 2013 to September 2015, he was appointed the College of Engineering Associate Dean for Academic Affairs. He is currently a Professor with the Electrical Engineering Department and a Senior Assessment and Evaluation Specialist with the Academic Planning and Quality Assurance (APQA) Office, Qatar University. His current research interests include power electronics and electric drives, energy efficiency, renewable energy, electric vehicles, and smart grids.

NASSER AL-EMADI (Senior Member, IEEE) received the B.Sc. and M.Sc. degrees in electrical engineering from Western Michigan University, Kalamazoo, MI, USA, in 1989 and 1994, respectively, and the Ph.D. degree in power systems from Michigan State University, East Lansing, MI, USA, in 2000. He is currently the Assistant Vice President of Faculty Affairs with Qatar University, Doha, Qatar, and an Associate Professor with the Department of Electrical Engineering, Qatar University. He has wide experience in electric power systems, control, protection, and sensor interfacing, control of multiphase motor drives, and renewable energy sources, and the integration of smart grids. He is a Founding Member of the Qatar Society of Engineers and a member of the Advisory Board of the IEEE Qatar Section.

MOHAMED DJEMAI (Senior Member, IEEE) received the master's degree in electrical engineering from the Ecole Nationale Polytechnique of Algiers, Algeria, in 1991, and the Ph.D. degree in control engineering from the CNRS-LSS, University of Paris XI, France, in 1996. He has been a Full Professor with the University of Valenciennes and Hainaut-Cambresis, Valenciennes, France, since 2008. He was a Visiting Professor with Northumbria University, from 2010 to 2013. He is currently with the Laboratory of Industrial and Human Automation, Mechanics and Computer Science, CNRS, UMR 8201. His current research interests include nonlinear control, observation, and fault detection theory, including hybrid system control, sliding-mode, and variable structure systems, with applications to power systems, robots, and vehicles. He is a member of IFAC TC 2.1 on control systems and IFAC TC. 1.3 on discrete event and hybrid systems.